crystals

MDPI

Article

High Thermal Stability and Color Purity of $Y_2SrAl_4SiO_{12}$: Eu^{3+} Garnet-Variant-Structured Phosphor for Warm White Light LED-Lamp

Xinhua Chen [1], Qingliang Xu [1], Fayaz Hussain [2], Chen Yang [1], Weiqin Sheng [1], Xinjiang Luo [1], Bing Liu [1], Shikuan Sun [3,*], Dawei Wang [4] and Kaixin Song [1,*]

1 College of Electronics Information, Hangzhou Dianzi University, Hangzhou 310018, China
2 Department of Materials Engineering, NED University of Engineering and Technology, Main University Road, Karachi 75279, Pakistan
3 School of Material Science and Energy Engineering, Foshan University, Foshan 528000, China
4 Functional Materials and Acousto-Optic Instruments Institute, School of Instrumentation Science and Engineering, Harbin Institute of Technology, Harbin 150080, China
* Correspondence: shikuansun@fosu.edu.cn (S.S.); kxsong@hdu.edu.cn (K.S.)

Abstract: Red LEDs with a high color purity and high color rendering index are often used to compensate for the lack of red-light components in current white LEDs. Therefore, the new type of garnet-structured high color purity red phosphor $Y_{2-x}SrAl_4SiO_{12}$: xEu^{3+} was synthesized by the solid-state method. The band gap structure of the host matrix was studied through the DFT calculation and found that the matrix belongs to a direct band gap structure with a band gap size of 4.535 *ev*. The phosphor exhibits a wide excitation spectrum under the monitoring of 710 nm. The strongest excitation wavelength is 393 nm, and it exhibits bright red light under the excitation of 393 nm, and the emission peak positions are located at 570 nm, 597 nm, 613 nm, 650 nm, 710 nm and 748 nm, respectively, which are attributed to the $^5D_0 \rightarrow {}^7F_j$ of Eu^{3+} (j = 0–5) electronic transitions. In the crystal structure of $Y_2SrAl_4SiO_{12}$, Eu^{3+} occupies a symmetry site. The compositional changes and thermal studies found favorable at 20% mol. At this concentration, the luminescence intensity gradually weakened due to the Eu^{3+} electric multi-level interaction. It is worth noting that the emission intensity of $Y_2SrAl_4SiO_{12}$: 20%Eu^{3+} at 433 K can be maintained to 92% of that at 293 K. Finally, we combined it with the NUV chip and packaged it into a red LED with a color purity of up to 90% and a correlated color temperature of 1492 K. The high purity, low color temperature and thermal stability indicate that it has a place in LED applications.

Keywords: garnet structure; phosphors; thermal stability; high color purity

check for updates

Citation: Chen, X.; Xu, Q.; Hussain, F.; Yang, C.; Sheng, W.; Luo, X.; Liu, B.; Sun, S.; Wang, D.; Song, K. High Thermal Stability and Color Purity of $Y_2SrAl_4SiO_{12}$: Eu^{3+} Garnet-Variant-Structured Phosphor for Warm White Light LED-Lamp. *Crystals* **2022**, *12*, 1382. https://doi.org/10.3390/cryst12101382

Academic Editor: Pier Carlo Ricci

Received: 9 September 2022
Accepted: 24 September 2022
Published: 29 September 2022

1. Introduction

For decades, the awareness of energy saving and environmental protection has become stronger and stronger, which requires us to constantly look for low-energy consumption products for transformation. White light-emitting diodes have attracted much attention due to their advantages of energy saving, environmental protection and low energy consumption [1–3]. At present, the commercial white LEDs are mainly composed of blue light chips + YAG: Ce^{3+} yellow phosphors. Due to the lack of red-light components in the combined white light, the color temperature is high, the color rendering index is low and the blue-light component is so high that the white light emitted is colder, which is harmful to the eyes. A series of problems exist. Therefore, it cannot be used in the field of high-quality lighting. How to enhance the red-light component of WLEDs has received extensive attention [4,5]. There are various materials for synthesizing red phosphors, such as red phosphors based on sulfide or nitrogen oxides. The phosphors of these two systems have good luminescence properties, as in Y_2O_2S: Eu^{3+} phosphors with high color

purity [6]. However, the chemical properties of sulfide phosphors are unstable, easy to decompose at high temperatures and sulfides pollute surroundings. For oxynitride red phosphors, for example, $Sr_2Si_5N_8$: Eu^{2+} [7] and $CaAlSiN_3$: Eu^{2+} [8] have excellent thermal and chemical stability, but the preparation process is complicated and strict, which requires high-temperature and reducing atmosphere. Nonetheless, these conditions hinder its commercial viability. Due to these limitations, the garnet structure is considered to be an effective host material for the fabrication of phosphors [9–11]. Garnet-structured aluminate phosphors have the advantages of high luminous efficiency, high thermal stability, simple preparation and environmental protection. Using the garnet structure as the matrix, phosphors made of different rare earth and transition elements can produce a variety of luminescence, such as $Tb_3Al_5O_{12}$: Eu^{3+} [12], YAG: Ce^{3+} [13], YAG: Dy^{3+} [14] and YAG: Mn^{4+} [15]. When sintered in air, Eu will exist in the matrix in the form of Eu^{3+}, which is one of the most widely used elements in red phosphor materials. At present, researchers have carried out a lot of research on the luminescence of Eu^{3+}. For example, Wang [16] et al. prepared the series of $Ca_2YZr_2Al_3O_{12}$: Eu^{3+} red phosphors, exhibiting typical red emission at 611 nm and brightness better than commercial Y_2O_3: Eu^{3+} phosphors. The fabricated compositions have lower color temperature (4745 K) and higher color rendering index (i.e., 86.72), which have potential applications in WLEDs electronics. Li [17] et al. prepared the $Ca_2GdHf_2Al_3O_{12}$: Eu^{3+} garnet-structured red phosphors using the high-temperature solid-phase method. It is excited at 394 nm and exhibits a typical Eu^{3+} emission band with a peak at 616 nm. When the temperature exceeds 200 °C, the Eu^{3+} emission intensity remains at 70.2% of that at initial temperature (−75 °C). Based on the above studies, it can be seen that how to improve the luminescent properties and thermal stability of red phosphors has always been a research hotspot and aluminosilicate garnet-structured phosphors are undoubtedly a good choice.

2. Experimental Procedures

$Y_2SrAl_4SiO_{12}$: xEu^{3+} (x = 0.05–0.35) series of samples were synthesized by the solid-state reaction method, with the raw materials of Y_2O_3 (99.99%, Aladdin), $SrCO_3$ (99.95%, Aladdin), Al_2O_3 (99.99%, Aladdin), SiO_2 (99.99%, Aladdin) and EuO (99.99%, Aladdin). The raw materials were weighed in stoichiometric proportions, then mixed with an appropriate amount of ethanol (95%) using an agate mortar and pestle and thoroughly ground. After drying, the mixture was transferred to an alumina oxide crucible and then sintered in a tube furnace by heating to 1450 °C for 10 h, followed by furnace-cooling to room temperature. Finally, the sintered samples were completely ground into powders for characterization of XRD and photoluminescence properties.

The crystal structure of the sintered samples was analyzed by an X-ray diffractometer (XRD, Rigaku, Ultima IV, Japan) with Cu-Ka radiation (wavelength = 5.66 nm), operated at 40 kV and 30 mA; where the scanning rate was 8° min^{-1} with 2θ range from 10° to 80°. The photoluminescence (PL) and photoluminescence excitation (PLE) spectra were measured by a Spectro-fluorometer system (Fluorlog-3, HORIBA JOBIN YVON, Paris, France) equipped with a 450-Watt Xe-lamp. The luminescence properties under different temperatures were measured by the standard phosphor thermal quenching analysis system (EX-1000, Hangzhou Ever Fine Co. Ltd., Hangzhou, China). The spectrum and performance test of WLEDs devices measured using LED light, color and electricity comprehensive testing instrument (HP9000, Hangzhou Hongpu Optoelectronics Technology Co., Ltd., Hangzhou, China).

3. Results and Discussion

The pure phase of YSAS: xEu^{3+} (x = 0.05–0.35) series phosphors was characterized by XRD, shown in Figure 1a. It can be seen that all the crystal planes (211, 400, 420, 422, 611, 640, 842, etc.) are well-matched with the standard alignment card PDF#88-2048, and no secondary phases composed of Eu^{2+} were detected in any of the samples, which indicated that Eu^{3+} was completely dissolved into the lattice of the YSAS matrix. With the increase in

Eu^{3+} concentration, the main diffraction peak shifts to a lower angle, which is caused by the ionic radius of Eu^{3+} being larger than that of Y^{3+} [18]. Figure 1b shows the crystal structure diagram. In the YSAS matrix, Y ions share a dodecahedral structure with Sr ions, Al^{3+} has two coordination environments, hereinafter referred to as Al1 and Al2, Al1 sites occupy an octahedral structure and Al2 shares a tetrahedral structure with Si. Since the ionic radius and valence state (CN = 8, R = 1.066 Å) of Eu^{3+} are similar to those of Y^{3+} (CN = 8, R = 1.019 Å) [19,20], Eu^{3+} can take the place of Y^{3+} and combine with eight oxygen atoms to form a dodecahedron. For the study of the energy band structure of the matrix, we used the density functional (DFT) method to calculate the energy band structure of YAG and YSAS and analyzed the band gap difference between them. As shown in Figure 1c,e, the band gap of YAG is 4.535 eV, while that of YSAS is 4.874 eV. It can be speculated that the incorporation of Sr-Si ions will promote the increase in the band gap effect. However, both substrates belong to the direct band gap structure because the conduction band bottom and the valence band top are located at the G point. Further, understand the band structures as shown in Figure 1d,f; their total density of states and partial density of states were calculated. From the density of states diagram, it can be seen that the top of the valence band of YAG is mainly composed of the O 2s states, and the bottom of the conduction band is mainly composed of the Y 4d states, Al 3s and 3p states. In the YSAS structure, the top of the valence band is mainly composed of the O 2s states, Al 3s states, Sr 5s states and Si 3p states, and the bottom of the conduction band is mainly composed of the Y 4d stats, Sr 3d states and 2p and 3s states of O. These results suggest that the intrinsic absorption of YSAS mainly originates from the charge transfer from the Al 3s states to the O 2p state.

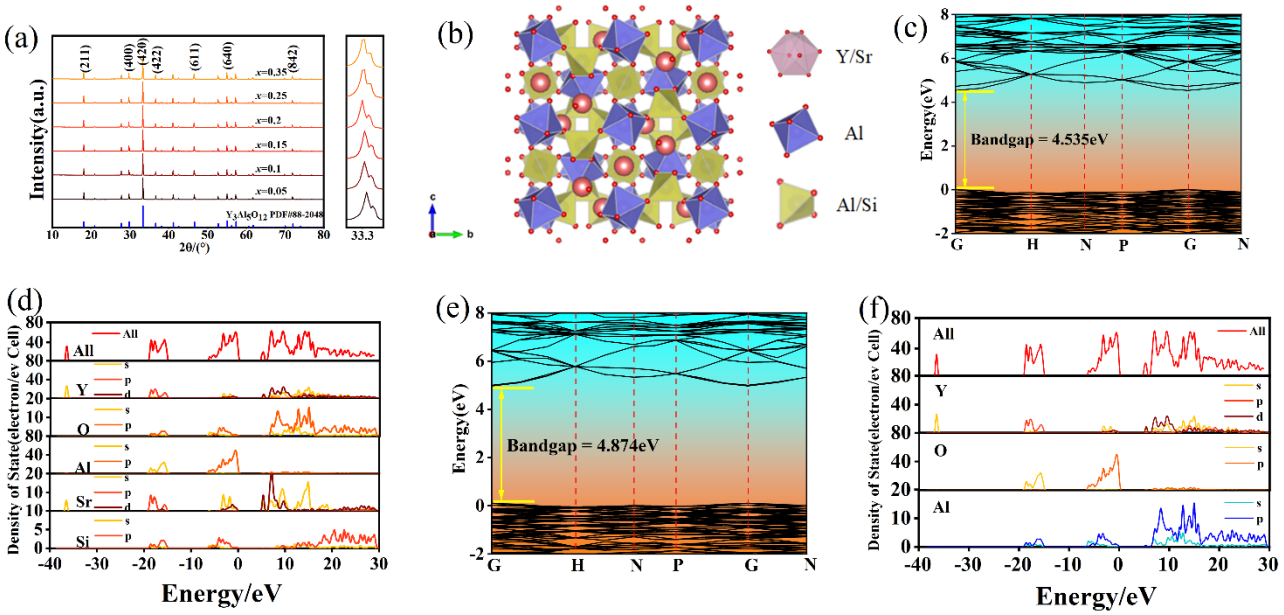

Figure 1. (**a**) YSAS: xEu^{3+} (x = 0.05–0.35) phosphor XRD pattern; (**b**) crystal structure; (**c**) YAG band structure; (**d**) density of states of YAG; (**e**) YSAS band structure; (**f**) density of states of YSAS.

In order to further study the structure of the samples, the structure was refined for YSAS at different Eu^{3+} concentrations by Rietveld analysis. Therefore, Figure 2a shows the refined image of YSAS: 0.15Eu^{3+}, and the refined data of other concentrations, further can be referred from the Supplementary Material data. The refinement parameters are all less than 10%, which can be considered as the reliability of the refinement results. Figure 2b shows the change in unit cell volume and unit cell parameters. It can be seen that the increases in Eu^{3+} content, the unit cell volume and unit cell parameters show an upward trend. This is because the ionic radius of Eu^{3+} is slightly larger than that of Y^{3+}. This also shows that Eu^{3+} successfully replaced the Y^{3+} lattice site.

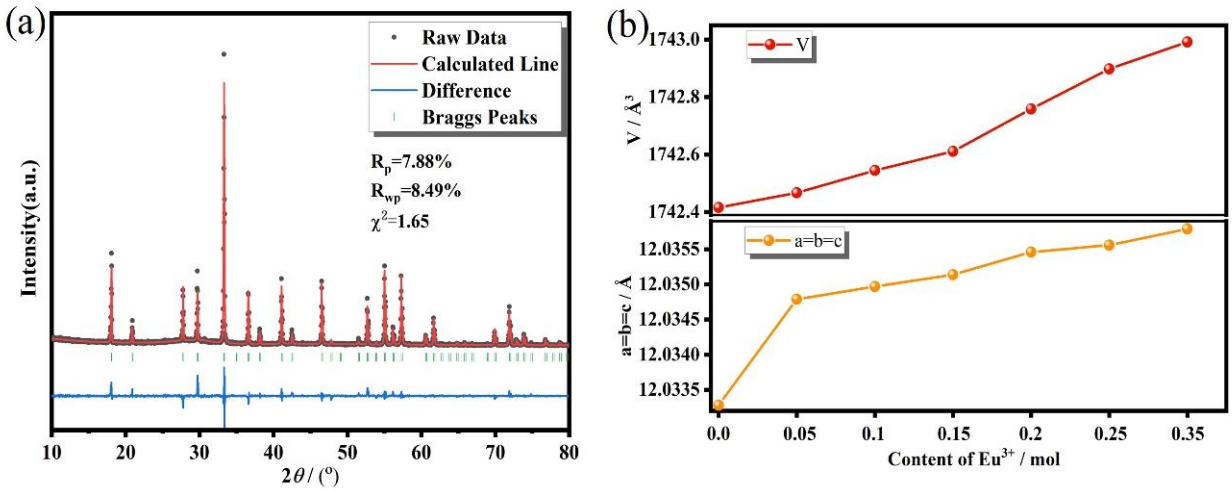

Figure 2. (**a**) YSAS: 0.15Eu^{3+} refined structure diagram; (**b**) variation in cell volume and lattice parameters with Eu^{3+} doping concentration.

To understand the composition of the sample spectrum, the excitation and emission spectra of the YSAS: 0.2Eu^{3+} sample were measured, as shown in Figure 3a. At a monitoring wavelength of 710 nm, the excitation spectrum exhibits a series of peak excitations from 350 to 550 nm. Among them, the peaks at 362, 381, 393, 412, 457 and 525 nm correspond to the transitions of Eu^{3+} from $^7F_0 \rightarrow {}^5D_4$, $^5G_2$, $^5L_6$, $^5D_3$, $^5D_2$ and $^5D_1$, respectively [21]. The strongest peak excitation is located at 393 nm, which can be efficiently excited by the near-ultraviolet chip. Under the most intense excitation at 393 nm, the emission spectrum of the sample consists of a series of peak emission from 550 to 750 nm. Among them, the sharp peaks at 578, 590, 612, 650, 710 and 748 nm originate from the electronic transition of Eu^{3+} from $^5D_0 \rightarrow {}^7F_j$ (j = 0–5), respectively. According to the excitation and emission spectra of YSAS: Eu^{3+} phosphors, the energy level transition diagram of Eu^{3+} in the host YSAS is drawn, as shown in Figure 3b. Under excitation at 393 and 461 nm, electrons can absorb energy transitions from the ground state ($^7F_0$) to the higher energy $^5L_6$ and $^5D_2$ excited levels. Due to the presence of nonradiative transitions, the higher state of the two energy levels to the lower $^5D_0$ energy level via a relaxation transition. Subsequently, the electrons at the $^5D_0$ level release energy in the form of photons to return to the ^7F_j (j = 0–5) ground state. It is worth noting that $^5D_0 \rightarrow {}^7F_1$ of Eu^{3+} belongs to the magnetic dipole transition and is not easily affected by the crystal field environment around Eu^{3+}, while $^5D_0 \rightarrow {}^7F_2$ belongs to the electric dipole transition, and the emission intensity is greatly affected by the crystal field environment where Eu^{3+} is located. It is well-known that the symmetry of the luminescent site of Eu^{3+} can be measured by the ratio of the emission intensity ($^5D_0 \rightarrow {}^7F_2$)/($^5D_0 \rightarrow {}^7F_1$) (the so-called R/O ratio). If the ratio R/O is less than one, it means that Eu^{3+} is in symmetry surroundings. If the ratio is greater than one, it indicates an asymmetric structure [22–24]. The phosphor YSAS in this paper: Eu^{3+}, $^5D_0 \rightarrow {}^7F_1$ and $^5D_0 \rightarrow {}^7F_2$ transitions are located at 597 nm and 613 nm, 630 nm, respectively. It can be seen from Figure 3c that the R/O of all concentrations is greater than one, indicating that Eu^{3+} is in an asymmetric environment in the host matrix.

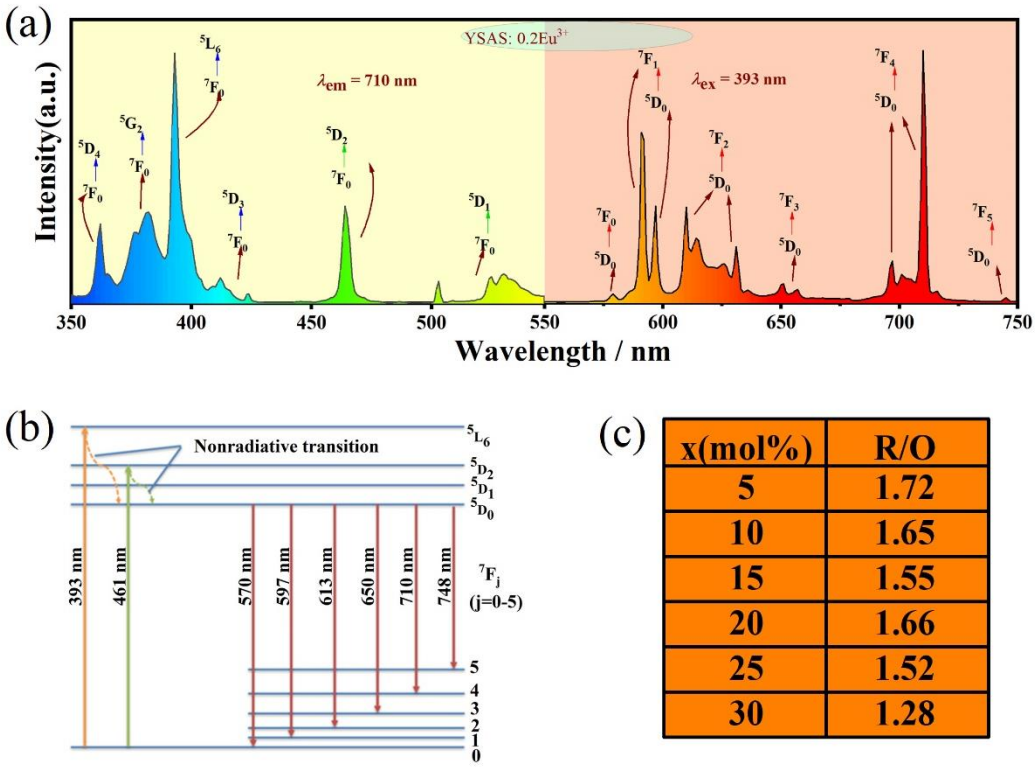

x(mol%)	R/O
5	1.72
10	1.65
15	1.55
20	1.66
25	1.52
30	1.28

Figure 3. (**a**) Excitation and emission spectra of YSAS: 0.2Eu^{3+}; (**b**) energy level structure diagram; (**c**) symmetry of Eu^{3+} in YSAS: xEu^{3+}.

Figure 4a is YSAS: the emission spectrum of xEu^{3+} series phosphors doped with different Eu^{3+}. Under the excitation at 393 nm, it can be seen that the overall luminescence intensity first increases and then decreases, reaches a maximum at x = 0.2 and finally, decreases due to concentration quenching. There are two main peaks in the emission spectrum: one is the peak at 597 nm, originating from the $^5D_0 \rightarrow {}^7F_1$ transition of Eu^{3+}, and the other is the peak at 710 nm, originating from the $^5D_0 \rightarrow {}^7F_4$ transition of Eu^{3+}. In order to clearly see the changes in these two main peaks, Figure 4b,c plot the changes in the two peaks with the intensity of Eu^{3+} doping concentration, both of which show a trend of first increasing and then decreasing. It reaches a maximum at x = 0.2 and then decreases due to concentration quenching. The critical distance can be evaluated by the following Formula (1) [25,26]:

$$Rc \approx 2\left(\frac{3V}{4\pi x_c N}\right)^{\frac{1}{3}} \quad (1)$$

where V represents the volume of the unit cell; X_c is the critical concentration of the activator ion; N is the number of cations in the unit cell. For the studied samples, V = 1742.467~1742.992 Å^3, x_c = 0.15~0.35, N = 8, the critical distances in the samples are calculated to be 10.59~20.26 Å. When the distance is greater than 5 Å, the electric multi-level interaction is effective. In addition to this, the interaction type can be obtained from Dexter's Formula (2) [27]:

$$\frac{I}{x} = \frac{k}{1+\beta(x)^{\frac{\theta}{3}}} \quad (2)$$

where x is the critical concentration of Eu^{3+}, I represents the luminescence intensity and k and β are constants. The fitting curves of $\lg(I/x)$ and $\lg(x)$ are shown in Figure 5 below. The fitted slope is -0.8028, so θ = 2.4. The obtained value of θ is closer to 6, so the reason for the concentration quenching of Eu^{3+} is due to the dipole–dipole interaction.

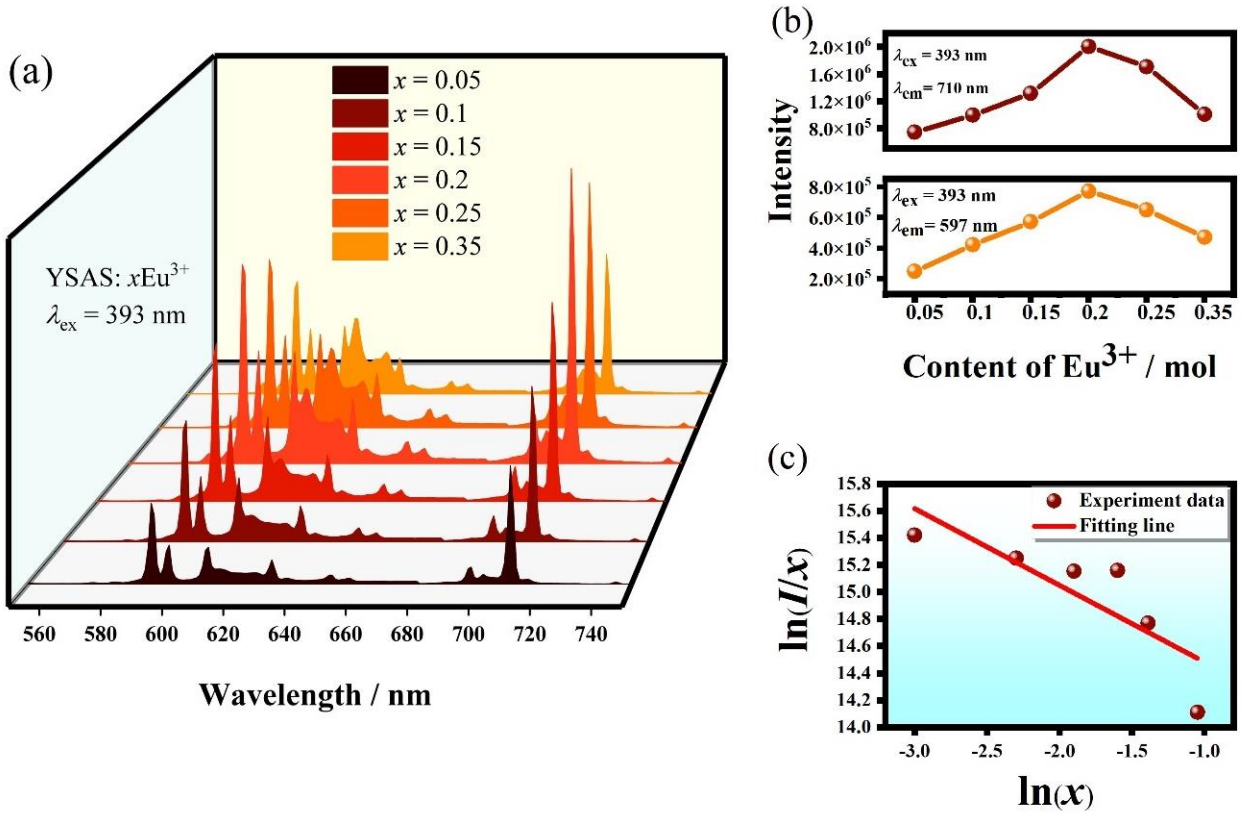

Figure 4. (**a**) Emission spectrum of YSAS: xEu^{3+} (λ_{ex} = 393 nm); (**b**) luminescence intensity at 710 nm and 597 nm; (**c**) linear fitting diagram of ln(x) and ln(I/x) of YSAS: xEu^{3+} (x = 0.05–0.35) series phosphors excited at 393 nm.

Thermal stability is an important property to determine whether a phosphor can be commercialized, as thermal stability of YSAS: $0.2Eu^{3+}$ phosphors is shown in Figure 5a. Since the characteristic emission of Eu^{3+} is linear, only a linear trend of intensity variation can be seen from Figure 5a. In order to get more intuitively preset the percentage of intensity relative to room temperature, Figure 5b shows that the luminescence intensity of Eu^{3+} at 710 nm decays with the increase in temperature. It can be seen that the luminescence intensity at 493 K can still maintain 93% of that at 293 K, indicating excellent thermal stability. The excellent thermal stability of phosphors depends on their activation energy ΔE, which can be calculated by the Arrhenius Formula (3) [28]:

$$I_T = \frac{I_0}{1 + A\exp\left(\frac{-\Delta E}{kT}\right)} \quad (3)$$

Among them, I_T represents the luminescence intensity at T temperature, I_0 represents the initial luminescence intensity, A is a constant, K is the Boltzmann constant (8.617×10^{-5} eV K^{-1}) and ΔE represents the activation energy of thermal quenching. In the inset of Figure 5b, the relationship between $\ln(I_T/I_0 - 1)$ and $1/kT$ is plotted, with the negative of the slope being the desired activation energy ΔE, which is 0.28713 eV. Generally, the thermal stability of phosphors is positively correlated with the activation energy [29], so larger activation energy leads to better thermal quenching performance of YSAS: $0.2Eu^{3+}$ phosphors. In order to further analyze the thermal quenching mechanism of phosphors, Figure 5c presents the configuration coordinate diagram. Under normal circumstances, after the electrons in the ground state are excited at 393 nm, they transition to the excited state $^5L_6$ and then go to $^5D_0$ through a nonradiative transition and finally, return to the ground state through a radiative transition. With the increase in temperature,

the excited electrons will overcome the barrier of activation energy and move to the CTB (charge transfer band transition), and finally, return to the ground state by nonradiative transition, which weakens the emission of Eu^{3+}. YSAS: The CIE chromaticity diagram of xEu^{3+} (x = 0.05–0.35) series phosphors is calculated under the excitation of 393 nm. It can be seen in Figure 5d that the coordinates of all samples fall in the CIE chromaticity diagram within the red area.

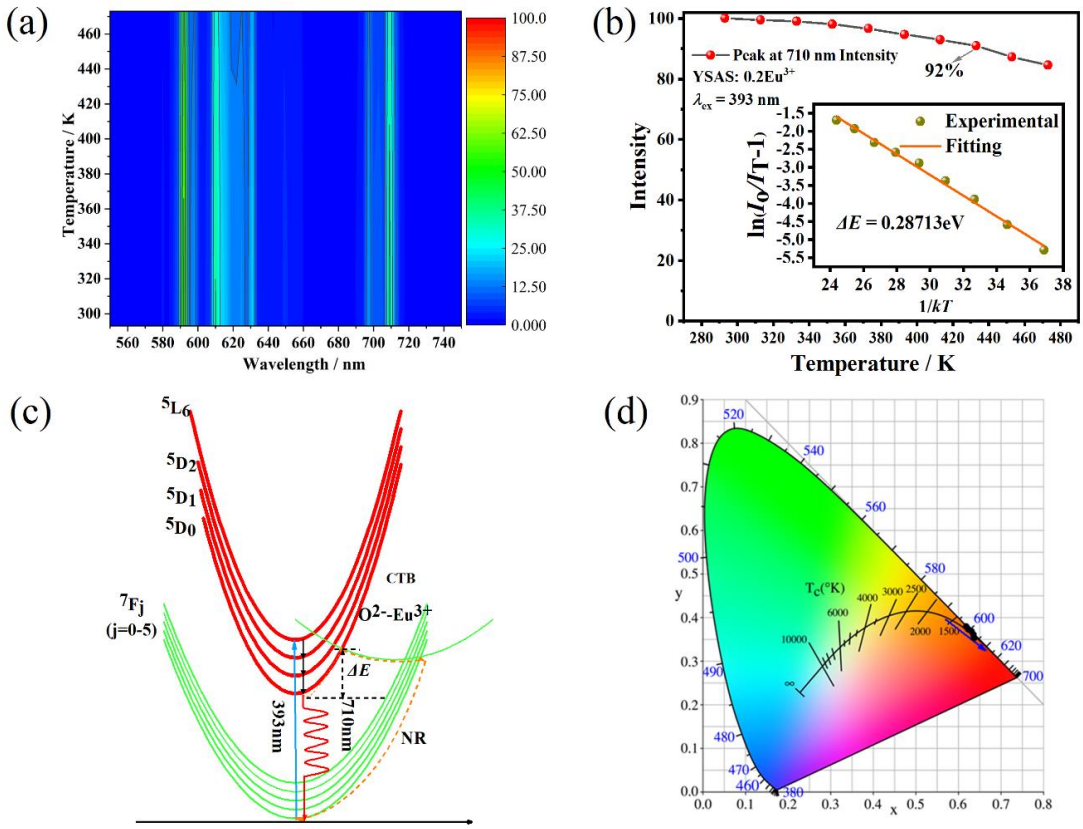

Figure 5. (**a**) YSAS: $0.2Eu^{3+}$ fluorescence intensity in the range of 293 K−473 K as a function of temperature (λ_{ex} = 393 nm); (**b**) 590 nm and 750 nm emission peak positions as a function of temperature (λ_{ex} = 393 nm); the calculated activation energy ΔE of YSAS: $0.2Eu^{3+}$ is shown in the inset; (**c**) schematic diagram of simple configuration coordinates of Eu^{3+}; (**d**) YSAS: CIE diagram of xEu^{3+} (x = 0.05–0.35) series phosphors excited at 393 nm.

Table 1 shows the thermal stability of Eu^{3+}-doped phosphors of different materials. It can be seen that the phosphors in this paper have great advantages in thermal stability, indicating that they have certain application prospects in the field of high power and high brightness.

Table 1. Thermal decay of Eu^{3+} phosphors in various compositions.

Materials	Thermal Decay Ratio (%)	Temperature (K)	ΔE (eV)	Ref
$Y_3Al_5O_{12}$	85.2	303→423	0.207	[30]
$Li_5La_3Ti_2O_{12}$	75	293→423	0.42	[31]
$CaTiO_3$	70	293→423	0.28452	[32]
$Li_5La_3Ta_2O_{12}$	63	293→423	0.20	[33]
Sr_2LaNbO_6	62.99	303→423	0.25	[34]
Ca_2YTaO_6	61	303→423	0.13	[35]
YSAS	92	293→433	0.28713	This work

The corresponding CIE color coordinates are shown in Table 2. YSAS: xEu^{3+} phosphor can display bright red light under the excitation of 393 nm. The CIE chromaticity coordinates (0.6390, 0.3606) of $Y_{1.8}Eu_{0.2}SrAl_4SiO_{12}$ phosphor are very close to the ideal red-light coordinates (0.670, 0.330). The corresponding color purity can be determined by the following Equation (4) [36]:

$$Color\ purity = \frac{\sqrt{(x - x_i)^2 + (y - y_i)^2}}{\sqrt{(x_d - x_i)^2 + (y_d - y_i)^2}} \times 100\% \quad (4)$$

Table 2. YSAS: CIE coordinates and CCT of xEu^{3+} (x = 0.05–0.35) series phosphors.

x	CIE (x, y)	Color Purity (%)	CCT (K)
0.05	(0.6247, 0.3748)	87.8	1902
0.1	(0.6289, 0.3706)	88.7	1974
0.15	(0.6318, 0.3678)	89.4	2030
0.2	(0.6346, 0.3650)	90.0	2092
0.25	(0.6359, 0.3637)	90.1	2123
0.35	(0.6390, 0.3606)	91.0	2204

Among them, x, y represent the CIE chromaticity coordinates of the sample; x_i, y_i represent the CIE chromaticity coordinates of white illumination (0.310, 0.316); x_d, y_d correspond to the color coordinates of the dominant wavelength (0.6747, 0.3251); the calculated color purity shown in Table 2, the results show that the phosphor has high color purity. The relevant color temperature can be calculated from the following Equation (5) [37]:

$$T = -437n^3 + 3601n^2 - 6861n + 5514.31 \quad (5)$$

Among them, the calculation method of n is as Equation (6):

$$n = \frac{x - 0.332}{y - 0.1858} \quad (6)$$

By calculation, the relevant color temperatures are shown in Table 1. It can be seen that the calculated color temperature is lower, all less than 2300 K. It shows that the YSAS: Eu^{3+} series phosphors can not only emit warm white light, but also have a lower color temperature.

Figure 6a shows the emission spectrum of the LED produced by YSAS: $0.2Eu^{3+}$ phosphor combined with NUV chip, driven by a current of 20 mA. The inset shows the appearance of the LED with and without the current applied. It can be seen that by applying a current of 20 mA, the LED emits a bright red light. In addition, the color temperature of this LED is CCT = 1492 K, which can be further combined with commercial green phosphors to make white LEDs with lower color temperature. Finally, Figure 6b shows the CIE coordinates of the red LED device. It can be seen that the coordinates are (0.4899, 0.2882), which is at the red light position.

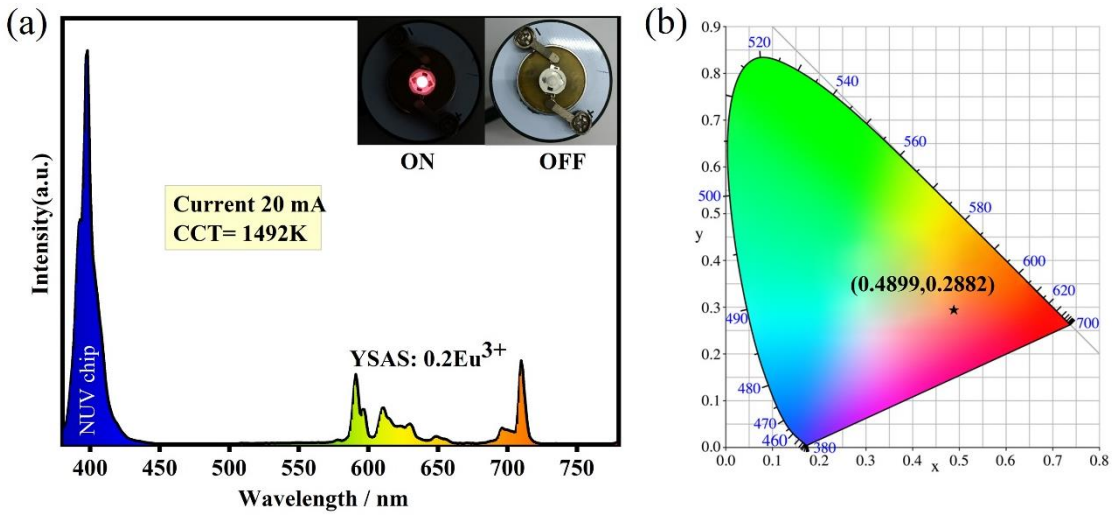

Figure 6. (**a**) PL spectrum of the LEDs device and (**b**) CIE coordinates diagram.

4. Conclusions

A series of YSAS: xEu^{3+} (x = 0.05–0.35) phosphor compounds were prepared by a solid-phase method, and the refined data indicated that Eu^{3+} successfully occupied the Y^{3+} site. Under the excitation of 393 nm, the sample exhibits a typical Eu^{3+} emission band, and the transition mode of each peak emission is studied in detail. Concentration quenching occurs due to the dipole–dipole interaction that occurs between Eu^{3+}. The relevant color purity was calculated by the CIE chromaticity coordinates diagram, which can reach 91% at x = 0.35. The emission intensity at 433 K remains at 92% of that at 293 K. The LED is encapsulated by combining with NUV chip, and the performance shows CCT = 1492 K, indicating that it can be a potential red phosphor for making white LED.

Supplementary Materials: The following supporting information can be downloaded at: https://www.mdpi.com/article/10.3390/cryst12101382/s1, Figure S1: (a)–(f) are the refined structures of YSAS: xEu^{3+}(x = 0.05–0.35) phosphors, respectively; Table S1: Refinement results of YSAS: xEu^{3+}(x = 0.05–0.35) phosphors.

Author Contributions: Conceptualization, X.C. and C.Y.; methodology, Q.X.; software, X.C.; validation, W.S. and D.W.; formal analysis, X.C.; investigation, S.S.; resources, K.S.; data curation, X.L.; writing—original draft preparation, X.C.; writing—review and editing, F.H. and K.S.; visualization, X.S.; supervision, B.L.; funding acquisition, K.S. All authors have read and agreed to the published version of the manuscript.

Funding: This research was funded by the National Natural Science Foundation of China under Grant No.: 51672063, 52161145401 and the Guangdong Key Platform & Programs of the Education Department of Guangdong Province for funding under Grant No. 2021ZDZX1003.

Institutional Review Board Statement: Not applicable.

Informed Consent Statement: Not applicable.

Data Availability Statement: Not applicable.

Acknowledgments: This work was supported by the National Natural Science Foundation of China under Grant No.: 51672063, 52161145401 and the Guangdong Key Platform and Programs of the Education Department of Guangdong Province for funding under Grant No. 2021ZDZX1003. We would also like to give thanks to NED University of Engineering and Technology, Department of Materials Engineering for research collaboration.

Conflicts of Interest: The authors declare no conflict of interest.

References

1. Qian, Y.; Zhu, D.; Pu, Y. A Zero-Thermal-Quenching Phosphor $Sr_3La(AlO)_3(BO_3)_4$: Dy^{3+} for Near Ultraviolet Excitation white-LEDs. *J. Lumin.* **2022**, *243*, 118610. [CrossRef]
2. Wang, J.; Guo, J.; Lv, Q.; Ma, Z.; Feng, X.; Lu, Y.; Gao, J.; Chen, W.; Deng, B.; Yu, R. Spectroscopic Investigation of the Novel Orange-Red Phosphor $Ca_3La_2W_2O_{12}$: Sm^{3+} with the High Color Purity for w-LED Applications. *J. Lumin.* **2022**, *241*, 118459. [CrossRef]
3. Shim, S.; Park, W.B.; Kim, M.; Lee, J.W.; Singh, S.P.; Sohn, K.S. Cyan-Light-Emitting Chalcogenometallate Phosphor, $KGaS_2$: Eu^{2+}, for Phosphor-Converted White Light-Emitting Diodes. *Inorg. Chem.* **2021**, *60*, 6047–6056. [CrossRef]
4. Huang, X.; Liang, J.; Rtimi, S.; Devakumar, B.; Zhang, Z. Ultra-High Color Rendering Warm-White Light-Emitting Diodes Based On an Efficient Green-Emitting Garnet Phosphor for Solid-State Lighting. *Chem. Eng. J.* **2021**, *405*, 126950. [CrossRef]
5. Liang, J.; Devakumar, B.; Sun, L.; Wang, S.; Sun, Q.; Huang, X. Full-Visible-Spectrum Lighting Enabled by an Excellent Cyan-Emitting Garnet Phosphor. *J. Mater. Chem. C* **2020**, *8*, 4934–4943. [CrossRef]
6. Yang, Z.; Yang, Y.; Li, X.; Li, X. Combustion synthesis of Y_2O_2S: Eu^{3+} phosphors. *ICO20 Mater. Nanostruct. SPIE* **2006**, *6029*, 441–446.
7. Yang, X.; Xing, X.J.; Liu, Y.F.; Mu, C.H.; Van Bui, H.; Zhang, Z.W.; Agathopoulos, S.; Xu, X.; Yin, L.J. A new thermal degradation mechanism of red Sr_2Si5N8: Eu phosphor: From the view of microstructural evolution. *Opt. Mater.* **2021**, *121*, 111506. [CrossRef]
8. Uheda, K.; Hirosaki, N.; Yamamoto, Y.; Naito, A.; Nakajima, T.; Yamamoto, H. Luminescence properties of a red phosphor, $CaAlSiN_3$: Eu^{2+}, for white light-emitting diodes. *Electrochem. Solid-State Lett.* **2006**, *9*, H22. [CrossRef]
9. Wang, M.; Cheng, T.; Dou, R.; Zhang, Q.; Jiang, H. Superior performance of a 2 kHz pulse Nd: YAG laser based on a gradient-doped crystal. *Photonics Res.* **2021**, *9*, 1191–1196.
10. Pan, Y.; Wu, M.; Su, Q. Tailored photoluminescence of YAG: Ce phosphor through various methods. *J. Phys. Chem. Solids* **2004**, *65*, 845–850. [CrossRef]
11. Tian, Y.; Chen, J.; Yi, X.; Jiang, R.; Lin, H.; Chen, L.; Zhou, S. Unravel the effect of lattice distortion on the 4f-5d excitation of Ce^{3+} in garnet phosphors. *J. Alloys Compd.* **2022**, *907*, 164412. [CrossRef]
12. Onishi, Y.; Nakamura, T.; Sone, H.; Adachi, S. Synthesis and properties of $Tb_3Al_5O_{12}$: Eu^{3+} garnet phosphor. *J. Lumin.* **2018**, *197*, 242–247. [CrossRef]
13. Ye, S.; Xiao, F.; Pan, Y.X.; Ma, Y.Y.; Zhang, Q.Y. Phosphors in phosphor-converted white light-emitting diodes: Recent advances in materials, techniques and properties. *Mater. Sci. Eng. R Rep.* **2010**, *71*, 1–34. [CrossRef]
14. Raju, G.S.R.; Jung, H.C.; Park, J.Y.; Chung, J.W.; Moon, B.K.; Jeong, J.H.; Son, S.M.; Kim, J.H. Sintering temperature effect and luminescent properties of Dy^{3+}: YAG nanophosphor. *J. Optoelectron. Adv. Mater.* **2010**, *12*, 1273–1278.
15. Chen, D.; Zhou, Y.; Xu, W.; Zhong, J.; Ji, Z.; Xiang, W. Enhanced luminescence of Mn^{4+}: $Y_3Al_5O_{12}$ red phosphor via impurity doping. *J. Mater. Chem. C* **2016**, *4*, 1704–1712. [CrossRef]
16. Wang, X.; Zhao, Z.; Wu, Q.; Li, Y.; Wang, Y. A Garnet-Based $Ca_2YZr_2Al_3O_{12}$: Eu^{3+} Red-Emitting Phosphor for n-UV Light Emitting Diodes and Field Emission Displays: Electronic Structure and Luminescence Properties. *Inorg. Chem.* **2016**, *55*, 11072–11077. [CrossRef]
17. Li, Y.; Wei, Q.; Chen, H.; Wang, Y. A Novel Red-Emitting $Ca_2GdHf_2Al_3O_{12}$: Eu^{3+} Phosphor for Light-Emitting Didoes and Field Emission Display. *J. Alloys Compd.* **2021**, *864*, 158840. [CrossRef]
18. Hussain, F.; Khesro, A.; Lu, Z.; Alotaibi, N.; Mohamad, A.A.; Wang, G.; Wang, D.; Zhou, D. Acceptor and donor dopants in potassium sodium niobate based ceramics. *Front. Mater.* **2020**, *7*, 160. [CrossRef]
19. Xia, Z.; Meijerink, A. Ce^{3+}-Doped garnet phosphors: Composition modification, luminescence properties and applications. *Chem. Soc. Rev.* **2017**, *46*, 275–299. [CrossRef]
20. Kadam, A.R.; Kohale, R.L.; Mishra, G.C.; Dhoble, S.J. Eu(III)-Doped Tri-Calcium $Ca_{3(1-X-Z)}M_Z(PO_4)_2A_X$: X Host Array: Optical Investigations of Down-Conversion Red Phosphor for Boosting Display Intensity and High Color Purity. *New J. Chem.* **2021**, *45*, 7285–7307. [CrossRef]
21. Gu, F.; Li, C.Z.; Jiang, H.B. Combustion synthesis and photoluminescence of MgO: Eu^{3+} nanocrystals with Li^+ addition. *J. Cryst. Growth* **2006**, *289*, 400–404. [CrossRef]
22. Wen, H.; Jia, G.; Duan, C.-K.; Tanner, P.A. Understanding Eu^{3+} emission spectra in glass. *Phys. Chem. Chem. Phys.* **2010**, *12*, 9933–9937. [CrossRef] [PubMed]
23. Ma, N.; Li, W.; Devakumar, B.; Huang, X. Dazzling Red-Emitting Europium (III) Ion-Doped $Ca_2LaHf_2Al_3O_{12}$ Garnet-Type Phosphor Materials with Potential Application in Solid-State White Lighting. *Inorg. Chem.* **2022**, *61*, 6898–6909. [CrossRef] [PubMed]
24. Yun, X.; Zhou, J.; Zhu, Y.; Li, X.; Liu, S.; Xu, D. A Potentially Multifunctional Double-Perovskite Sr_2ScTaO_6: Mn^{4+}, Eu^{3+} Phosphor for Optical Temperature Sensing and Indoor Plant Growth Lighting. *J. Lumin.* **2022**, *244*, 118724. [CrossRef]
25. Blasse, G. Energy transfer in oxidic phosphors. *Philips Res. Rep.* **1969**, *24*, 131. [CrossRef]
26. Van Uitert, L.G. Characterization of energy transfer interactions between rare earth ions. *J. Electrochem. Soc.* **1967**, *114*, 1048. [CrossRef]
27. Dexter, D.L. A theory of sensitized luminescence in solids. *J. Chem. Phys.* **1953**, *21*, 836–850. [CrossRef]
28. Laidler, K.J. The development of the Arrhenius equation. *J. Chem. Educ.* **1984**, *61*, 494. [CrossRef]

29. Chen, Y.; Shen, Y.; Zhou, L.; Lin, J.; Fu, J.; Fang, Q.; Ye, R.; Shen, Y.; Xu, S.; Lei, L.; et al. Temperature-dependent luminescence of Bi^{3+}, Eu^{3+} co-activated La_2MgGeO_6 phosphor for dual-mode optical thermometry. *J. Lumin.* **2022**, *249*, 118995. [CrossRef]
30. Yao, J.; Zhu, Q.; Li, J.G. Garnet transparent ceramic film of $Y_3Al_5O_{12}$: Eu^{3+} fabricated through an interface reaction of layered rare-earth hydroxide nanosheets on amorphous alumina. *Appl. Surf. Sci.* **2022**, *579*, 152226. [CrossRef]
31. Zhang, S.; Zhang, P.; Liu, X.; Yang, Z.; Huang, Y.; Seo, H.J. A red-emitting phosphor of $Li_5La_3Ti_2O_{12}$: Eu^{3+} with garnet-like structure and near-UV/blue light excitation. *J. Lumin.* **2018**, *203*, 152–159. [CrossRef]
32. Wu, Y.; Zhao, F.; Ruan, K.; Zhang, H.; Piao, X. Synthesis of (Ca, Zn) TiO_3: Eu^{3+} red phosphors via the sol–gel method and their luminescence properties. *Chem. Phys. Lett.* **2015**, *633*, 234–240. [CrossRef]
33. Liu, B.; Wang, K.; Li, J.; Liu, Z. The synthesis and luminescent properties of Eu^{3+} doped $Li_5La_3Ta_2O_{12}$ garnet phosphor with enhanced red emission and thermally stable. *J. Solid State Chem.* **2022**, *305*, 122658. [CrossRef]
34. Hua, Y.; Ran, W.; Yu, J.S. Excellent photoluminescence and cathodoluminescence properties in Eu^{3+}-activated Sr_2LaNbO_6 materials for multifunctional applications. *Chem. Eng. J.* **2021**, *406*, 127154. [CrossRef]
35. Huang, X.; Wang, S.; Liang, J.; Devakumar, B. Eu^{3+}-activated Ca_2YTaO_6 double-perovskite compound: A novel highly efficient red-esmitting phosphor for near-UV-excited warm w-LEDs. *J. Lumin.* **2020**, *226*, 117408. [CrossRef]
36. Wyszecki, G.; Stiles, W.S. *Color Science*; Wiley: New York, NY, USA, 1982.
37. McCamy, C.S. Correlated color temperature as an explicit function of chromaticity coordinates. *Color Res. Appl.* **1992**, *17*, 142–144. [CrossRef]